Rain Observations by a Multifrequency Dual-Polarized Radiometer

Alessandro Battaglia, Pablo Saavedra, Clemens Simmer, and Thomas Rose

***Abstract*—During the Convective and Orographically Induced Precipitation Study, advanced microwave radiometer for rain identification has continuously acquired measurements at the Atmospheric Radiation Measurement Mobile Facility in the Black Forest from the beginning of August until December 2007. The radiometer has six channels measuring in horizontal and vertical polarizations at 10.65, 21.0, and 36.5 GHz. Rainy events have been selected out of the entire database according to collocated gauges and, subsequently, analyzed. Measured brightness temperatures and (vertical–horizontal) polarization differences are interpreted by comparing with radiative transfer simulations, which account for the presence of nonspherical particles in preferential orientation. Measurements confirm the importance of the polarization signal for separating the effect introduced by non-Rayleigh scatterers and, therefore, the rain from the cloud component. More quantitative interpretation of the signal requires a better understanding of the role played by melting particles and an identification of the 3-D structure of the precipitating system under observation. Both aspects will be tackled in the near future by exploiting the synergy with a coinstalled micro rain radar.**

***Index Terms*—Ground-based remote sensing, microwave radiometry, radiative transfer, rainfall.**

I. Introduction

A LONG-TERM standing problem in cloud physics resides in the quantification of the rain efficiency, i.e., of the efficiency of a cloud in producing rain from cloud water, and in the identification of thresholds for the autoconversion of cloud droplets into raindrops. For a given amount of liquid water, clouds with a number concentration below a certain threshold are assumed to contain large-enough droplets to induce sufficient collision and coalescence to produce the embryonic raindrops necessary for precipitation development. On the other hand, no rainfall development is expected in clouds with higher concentration of small droplets because of a reduced frequency of collisions and a reduced coalescence efficiency between such droplets. An increase in the number of cloud droplets may potentially suppress the formation of precipitation, e.g., decreasing the rain efficiency [1]. This is particularly relevant for the so-called second indirect aerosol effect.

Manuscript received September 29, 2008; revised November 27, 2008. First published February 20, 2009; current version published April 17, 2009. This work was supported by Deutsche Forschungsgemeinschaft (DFG) under Grant BA 3485/1-1.

A. Battaglia, P. Saavedra, and C. Simmer are with the Meteorological Institute, University of Bonn, 53121 Bonn, Germany (e-mail: batta@uni-bonn.de; pablosaa@uni-bonn.de; csimmer@uni-bonn.de).

T. Rose is with Radiometer Physics GmbH, 53340 Meckenheim, Germany (e-mail: rose@radiometer-physics.de).

Color versions of one or more of the figures in this paper are available online at http://ieeexplore.ieee.org.

Digital Object Identifier 10.1109/LGRS.2009.2013484

The autoconversion processes are generally described by Kessler-type parameterizations in cloud modeling (e.g., [2]) but they have been never substantially validated by *in situ* or remote sensing measurements. This leaves some fundamental open questions.

1) *Is it true that a cloud with high concentration of CCN (e.g., higher than 400* cm^{-3}*) can support cloud liquid-water contents up to* 0.8–1 $\mathrm{g/m}^3$ *before precipitating?* Such high values have been hypothesized by Berg *et al.* [3] in order to explain some Tropical Rainfall Measuring Mission (TRMM) observations over west China (see [3, Figs. 4 and 5]) with no detectable precipitation-radar echoes but with a strong TRMM Microwave Imager signal.
2) *How does the ratio of the rain liquid-water path to the cloud liquid-water path (R-LWP, C-LWP, hereafter) change for different rain clouds?* In cloud modeling, large uncertainties are still present in such partitioning as shown in [4, Fig. 11]: while the unified microwave ocean retrieval algorithm assumes an analytical relationship between the two quantities based on the model of [5], the Goddard profiling algorithm, based on cloud resolving simulations, assumes a totally different distribution. However, no disproof/validation of any of such models has been proposed up to now.

Remote sensing instruments have severe problems in partitioning cloud from precipitating particles or in identifying the onset of precipitation. Radars are sensitive to the sixth moment of the drop radius; thus, their signal is always dominated by the largest drops in the sampling volume. On the other hand, microwave radiometry is a fairly established technique to retrieve vertically integrated C-LWP with dual-channel radiometers with an estimated accuracy of up to 15 $\mathrm{g/m}^2$ (e.g., [6]). However, above $\sim$300 $\mathrm{g/m}^2$, clouds generally contain raindrops that will undergo the following conditions: 1) may wet the receiving antenna, thus producing absorption losses directly at the antenna window or at the reflector plate used to redirect the radiation into the radiometer feed window, and 2) break down the applicability of the Rayleigh approximation, according to which the extinction coefficient is essentially proportional to the mass of the particles so that the total optical thickness is directly proportional to the LWP. Cloud droplets produce a different mass extinction coefficient than raindrops because, in the Mie resonance region, the extinction cross sections remain higher than their Rayleigh counterpart. Therefore, the same amount of LWP appears "brighter" [i.e., produces higher brightness temperatures (T_B's)] when the rain component is dominant.

Fig. 1. ADMIRARI radiometer. On the right side, (black antenna) a micro-rain radar system is installed.

As a direct implication, in LWP retrieval, the rms and bias errors strongly increase in the presence of rain and can easily be higher than 100 g/m^2 even for total LWP less than 1 kg/m^2 [7]. Despite these problems, others [8]–[11] have focused on the potential of multiwavelength ground-based radiometer observations in retrieving integrated rain contents of precipitating clouds.

Czekala *et al.* [12] proposed multispectral ground-based measurements of vertical (T_B^V)- and horizontal (T_B^H)-polarized brightness temperature and polarization difference ($PD = T_B^V - T_B^H$) to enable the detection of rain initiation and to estimate rain/cloud partitioning. The underlying idea is that large raindrops have nonspherical shapes, which produce unique negative-polarization signatures when observed from a ground-based microwave radiometer; the amount of the effect mainly depends on the radiometer frequency, the vertical distribution of hydrometeors, and the observation slant angle. However, up to now, few ground-based polarized measurements at MW frequencies have been documented in literature. Only Czekala *et al.* [13] confirmed the presence of negative-polarization differences in ground-based observations with a single-frequency 19.2-GHz dual-polarization radiometer observing at 30° elevation angle.

The **AD**vanced **MI**crowave **RA**diometer for **R**ain **I**dentification (ADMIRARI) has been developed to fill this gap of measurements and to evaluate the information content added by polarization differences and by adopting a multispectral approach.

II. Description of the ADMIRARI Radiometer

ADMIRARI, manufactured by Radiometer Physics GmbH (www.radiometer-physics.de), comprises six channels: 10.65, 21.0, and 36.5 GHz, all with horizontal and vertical polarizations (see Fig. 1 and additional information at www.meteo.uni-bonn.de/forschung/gruppen/admirari). For the 21- and 36-GHz frequency modules, the receiver optics consists of a corrugated feed with an aperture lens, while at 10.65 GHz, the beam is formed by a combination of a corrugated feed horn and an off-axis parabola antenna; all 3 frequencies achieve an antenna beamwidth of 5°. The aperture lens (and the 10-GHz parabola) are coated by a water-repellent film to avoid the sticking of raindrops on them; they are also equipped by a shield which is effective in protecting the lens from rain when the radiometer is measuring at low elevation angles. A radiometer accuracy better than 0.4 °C RMS at 1.0-s integration time is achieved with an absolute system stability of 1.0 K. The system is fully steerable both in azimuth (0°–360°) and in zenith (−90°–90°), and for easy transportation, it is mounted on a trailer.

III. Measurements During the COPS Campaign

As part of the Convective and Orographically Induced Precipitation Study (COPS) (for a full description, see [14]), the ADMIRARI radiometer was deployed at the ARM Mobile Facility in the Murg Valley, Black Forest, south Germany. This offers the opportunity to integrate the ADMIRARI measurements with other instruments present at the measuring site (e.g., the AMF meteorological station including a rain gauge, radiosondes, and the vertically pointing W-band radar).

ADMIRARI has been continuously measuring from August 8 to December 19. The basic scanning strategy adopted during the campaign consists of a 15-min cycle subdivided into an 8-min-long constant 30° elevation observation mode and an elevation scan at a fixed azimuth direction for 4 min, plus a zenith mode for the remaining 2 min. The focus of this letter is on the observations at the fixed 30° elevation angle where strong polarization signals are expected.

An example of a daily measurement is shown in Fig. 2. September 18 was characterized by a series of rain events with the first part of the day dominated by stratiform events with different convective events occurred during the afternoon. A peak of 45 mm/h was reached around 4:00 A.M., corresponding to a stratiform-embedded convective event which attenuates strongly the radar signal. Freezing level descended during the day from around 3–1.5 km. Between 7:30 and 10:00 A.M., radiometer data are not displayed because of intense electromagnetic interferences at the measuring site. The T_B's ($T_B = (1/2)(T_B^V + T_B^H)$) shows a strong correlation with the rain rate (as expected) but with a frequency-dependent dynamic range: The 10-GHz channel is basically never exceeding 110 K with a clear-sky baseline around 8 K while 21 GHz (36.5 GHz) T_B's range between 45 and 240 K (277 K). This is obviously due to the larger opacity of the atmosphere at higher frequencies. The polarization differences show negative values in the presence of rain in agreement with expectations. However, the amplitude of this signal does not follow in general the T_B's. For instance, although having similar T_B's at 21 and 36 GHz, the two peaks at 11:00 A.M. and at 11:30 A.M. present different PDs. According to the theory [12], this should be a sign of the presence of a higher fraction of rain versus cloud water in the scanned volume at 11:30 A.M. At 36.5 GHz, the PD signal is generally lower, with the largest negative values not achieved in parallel with the highest T_B's. This is a result of the saturation effect when large optical thicknesses (≥ 4) are sensed, i.e., of the counterbalancing between emission (due to their preferential horizontal alignment, raindrops tend to

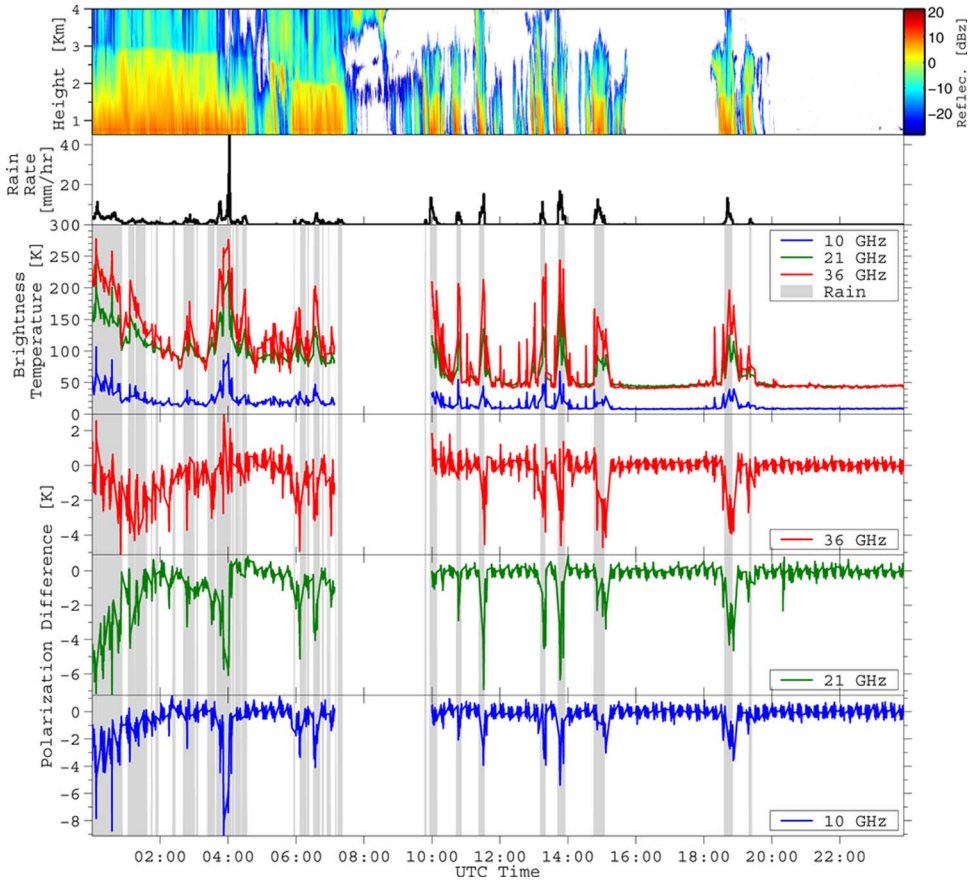

Fig. 2. Examples of measurements for September 18, 2007. From top to bottom: W-Band radar reflectivity, gauge rain rate, brightness temperatures ($T_B = (1/2)(T_B^V + T_B^H)$), and 36.5-, 21-, and 10.65-GHz polarization difference ($PD = T_B^V - T_B^H$), respectively, for azimuth scan at 30° elevation. Gray intervals indicate rainy periods as sensed by the gauge at the ARM site.

emit more H- than V-polarized radiation, thus producing negative PDs) and propagation effects (raindrops attenuate more H-radiation, thus letting more V-radiation reach the receiver). In some cases, for very high T_B's (like at 4:00 A.M., PDs even become positive. This effect has been predicted in the frame of 3-D effects [15]. Finally, note that PDs have a typical noise level around 0.5 K.

The whole COPS data set has been quality checked. Cases identified as rainy by the gauge have been further analyzed: for each frequency, (T_B, PD) occurrence plots are shown in Fig. 3. When looking at each frequency separately, results appear to be in agreement with theoretical expectations and with [12, Figs. 2 and 3]. At 10.65-GHz, T_B's never exceed 130 K, which roughly corresponds to a slant optical thickness of 0.65. On the other hand, at 36.5 GHz, values close to ambient ground temperature are reached, clear signatures of very thick atmospheres. For any given T_B, the variability of PDs is related to the relative presence of rain/cloud particles in the slant column under observation. In the presence of a large fraction of rain (cloud) content, the corresponding points are likely to be located in the lower (upper) branch of the colored contour in Fig. 3.

IV. Toward a Retrieval Algorithm: Open Issues

A retrieval algorithm capable of distinguishing between C-LWP and R-LWP is now under development. The algorithm is based on radiative transfer simulations, which use cloud resolving model hydrometeor profiles of precipitating systems. Five hydrometeor types are included: rain, cloud water, cloud ice, graupel, and snow. Raindrops are represented as horizontally oriented oblate spheroids with axial ratios (lower than one) parameterized according to [16]. The single-scattering properties (i.e., the extinction and the phase matrices and the emission vector) are computed according to [17]. In order to include 3-D effects, each precipitating profile, characterized by different horizontal extents (varied from 250 m to 8 km), is embedded in a clear-sky atmosphere. The radiances are then simulated as sensed by a radiometer with an antenna beamwidth of 5° located at different positions, either underneath the cloud or at the side of the cloud. The radiative transfer equation is solved according to the backward Monte Carlo technique [18]. An example of such simulations with freezing levels between 2 and 2.5 km (0.5 km is a reasonable estimate of the uncertainty in the determination of such a quantity during the campaign) is shown in Fig. 4. Triangles down, dots, squares, circles, pluses, pentagrams, hexagrams, triangles right, crosses, and triangles up correspond to slant total LWP between 0 and 0.5 kg/m^2, 0.5 and 1 kg/m^2, ..., 4.5 and 5 kg/m^2, respectively. The color of the symbols is modulated by the rain fraction (0% means pure cloud, 100% pure rain). Therefore, regions with the same color correspond to profiles with the same cloud/rain partitioning and regions with the same symbols to profiles with approximately

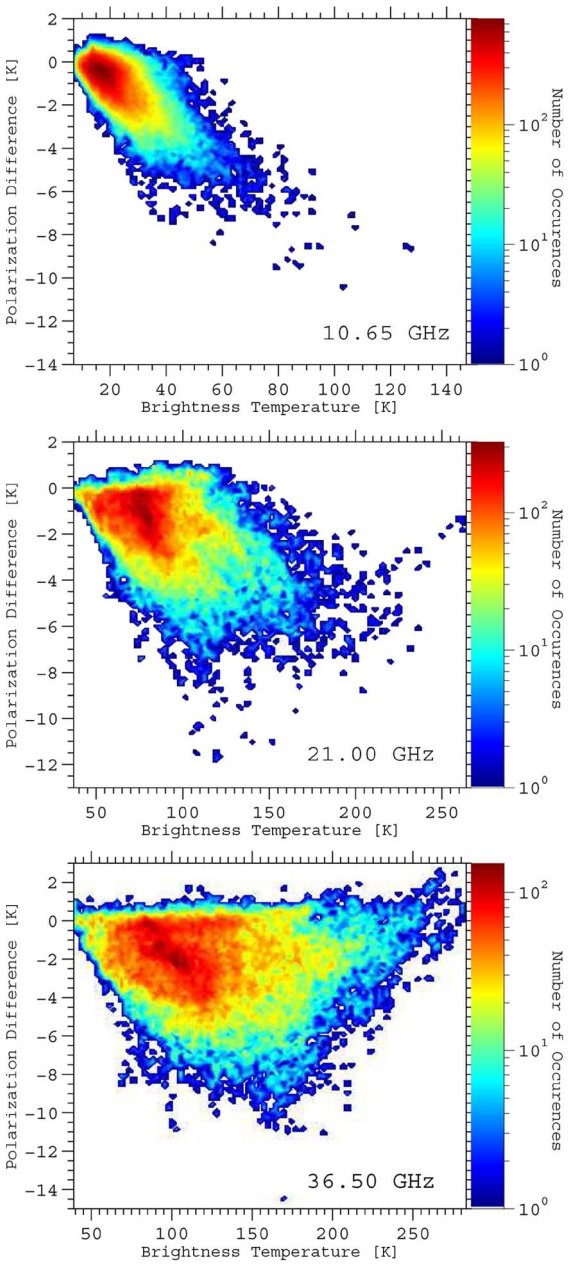

Fig. 3. Distribution of occurrences of measured (T_B's, PDs) in rainy conditions for the whole COPS campaign for the three ADMIRARI frequencies [(top) 10.65, (center) 21, and (bottom) 36.5 GHz]. Only azimuth scans at 30° elevation.

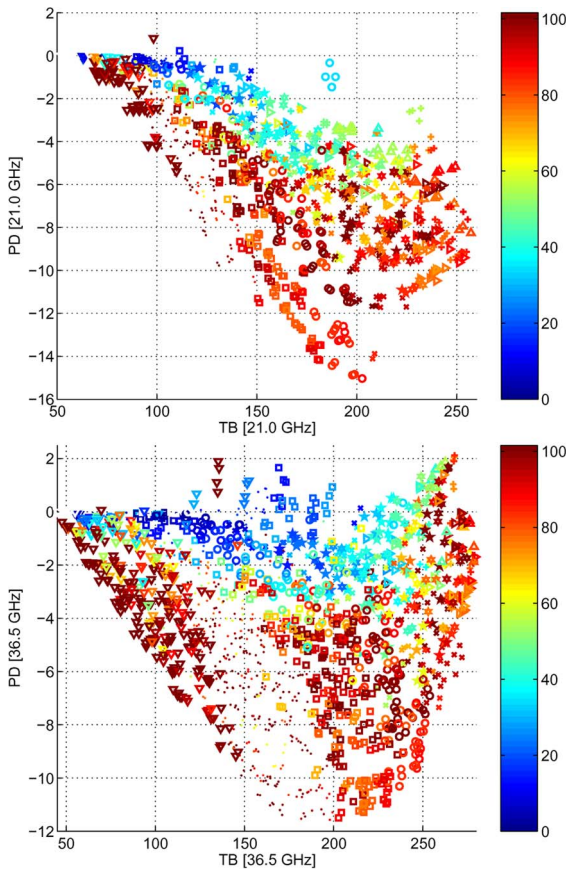

Fig. 4. Simulated (T_B's, PDs) at (top) 21.0 and (bottom) 36.5 GHz at 30° elevation angle. Only system with freezing levels between 2 and 2.5 km are considered. Triangles down, dots, squares, circles, pluses, pentagrams, hexagrams, triangles right, crosses, and triangles up correspond to slant total LWP from 0 to 5 kg/m^2 in steps of 0.5 kg/m^2, respectively. The color of the symbols is modulated by percentage of rain fraction (0% means pure cloud, 100% pure rain).

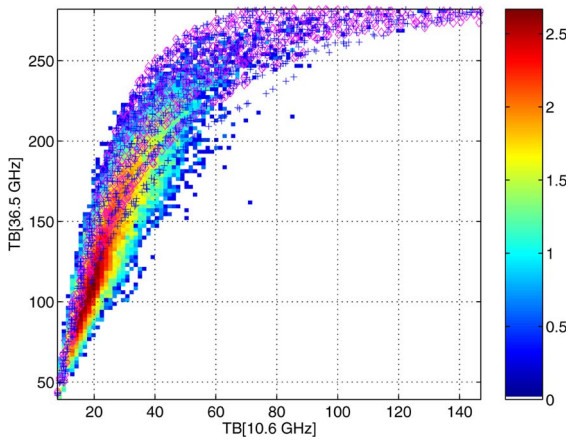

Fig. 5. (Crosses and diamonds) Simulated and measured T_B's for the 10.6- and the 36.5-GHz frequencies at 30° elevation angle. The color scale accounts for Log_{10} of the number of occurrences.

the same total slant LWPs. Note that, in this letter, due to the variability of the drop size distribution (here, we used exponential distributions with $N_0 = 4,\ 8,\ 32 \times 10^3 [\mathrm{m}^{-3} \cdot \mathrm{mm}^{-1}]$), to the 3-D configuration, to the vertical-profile unevenness, and to the presence of ice hydrometeors, the cloud/rain partitioning is not so well defined as in the simulations in [12]. Variations in raindrop axial ratio parameterizations only affect PDs, and the associated sensitivity is smaller than the effect caused by considered DSD changes. A complementary role is played by the two upper frequencies: 35.6 GHz is already sensitive to rain systems with slant LWP around 0.4–0.5 kg/m^2 and seems to be optimally suitable around 1.0 kg/m^2, while 21 GHz has a larger dynamic range for systems with total LWP around 1.5–2 kg/m^2.

Some pitfalls have been identified so far. In Fig. 5, which reproduces the scatter plot (10.6 T_B's versus 36.5 T_B's), the model results cannot capture the variability shown by measurements. In particular, modeled 10.6-GHz T_B's are systematically lower than measured ones. Similar results are found for (10.6 T_B's versus 21.0 T_B's). On the other hand, the variability

of the couple of T_B's at 21 and 36.5 GHz is well covered by the modeling (not shown). This requires further investigation; two possible explanations are under consideration.

1) The 10.6-GHz channels, different from the other channels, has an off-axis parabola antenna; this can produce biases due to different calibration procedures and wetting modalities.
2) No melting particles have been considered up to now in our modeling. When introduced, melting particles will introduce an excess of optical thicknesses at all frequencies. However, the relative effect is known to be higher at the lowest frequency (e.g., [19]), thus producing systematically higher T_B's enhancements at 10.6 GHz.

To have a better insight in such problems, the instrument has been equipped with a micro rain radar, manufactured by METEK (Meteorologische Messtechnik GmbH, www.metek.de), pointing at the same direction as the radiometer (see the black antenna on the right side of Fig. 1). The radar will be able to identify cases with bright band and will provide a better constraint to the inversion problem by ranging the rain component in the sensed volume. Then, the numerical-simulation assumptions can be further restricted and the ambiguities reduced. A Bayesian scheme which uses the three ADMIRARI T_B's, the three PDs, and the micro-rain radar reflectivity measurements in the levels below the freezing altitude in relation to the corresponding simulated quantities is currently under implementation.

V. Conclusion

In this letter, new-concept multiwavelength dual-polarized radiometric measurements have been acquired in the frame of COPS. Rain-coincident data show prevalence of H-polarized radiation with the extent of the polarization signal being strongly frequency-dependent. Each given T_B corresponds to a range of PDs, confirming the hypothesis that a variety of partitioning ratios between rain and cloud generally occurs in precipitating systems. Future work envisages to develop a retrieval scheme for the rain/cloud partitioning. To achieve such a goal, simulations have demonstrated that a more detailed description of the rain system under observations is mandatory. Bright-band identification and location of the rain components are considered as two key aspects and will be provided in a future field experiment by the synergy of our radiometer with an active frequency-modulated continuous-wave radar. Rain/cloud partitioning will provide ground-breaking feedbacks for cloud modelers toward a better characterization of rain processes.

Acknowledgment

The authors would like to thank the supervisors of the COPS supersite M. Data were obtained from the Atmospheric Radiation Measurement Program. The ADMIRARI radiometer was funded by DFG under Grant BA 3485/1-1.

References

[1] R. R. Rogers and M. K. Yau, *A Short Course in Cloud Physics*. Woburn, MA: Butterworth–Heinemann, 1989.
[2] Y. Liu and P. H. Daum, "Parameterization of the autoconversion process—Part I: Analytical formulation of the Kessler-type parameterizations," *J. Atmos. Sci.*, vol. 61, no. 13, pp. 1539–1548, Jul. 2004.
[3] W. Berg, T. L'Ecuyer, and C. Kummerow, "Rainfall climate regimes: The relationship of regional TRMM rainfall biases to the environment," *J. Appl. Meteorol.*, vol. 45, no. 3, pp. 434–454, Mar. 2006.
[4] K. A. Hilburn and F. J. Wentz, "Intercalibrated passive microwave rain products from the unified microwave ocean retrieval algorithm (UMORA)," *J. Appl. Meteorol.*, vol. 47, no. 3, pp. 778–794, Mar. 2008.
[5] F. J. Wentz and R. W. Spencer, "SSM/I rain retrievals within a unified all-weather ocean algorithm," *J. Atmos. Sci.*, vol. 55, no. 9, pp. 1613–1627, May 1998.
[6] S. Crewell and U. Löhnert, "Accuracy of cloud liquid water path from ground-based microwave radiometry—Part II: Sensor accuracy and synergy," *Radio Sci.*, vol. 38, no. 3, p. 8042, Feb. 2003. DOI: 10.1029/2002RS002634.
[7] U. Löhnert and S. Crewell, "Accuracy of cloud liquid water path from ground-based microwave radiometry—Part I: Dependency on cloud model statistics," *Radio Sci.*, vol. 38, no. 3, p. 8041, Feb. 2003. DOI: 10.1029/2002RS002654.
[8] G.-R. Liu, C.-C. Liu, and K. Tsung-Hua, "Rainfall intensity estimation by ground-based dual-frequency microwave radiometers," *J. Appl. Meteorol.*, vol. 40, no. 6, pp. 1035–1041, Jun. 2001.
[9] F. S. Marzano, D. Cimini, P. Ciotti, and R. Ware, "Modeling and measurements of rainfall by ground-based multispectral microwave radiometry," *IEEE Trans. Geosci. Remote Sens.*, vol. 43, no. 5, pp. 1000–1011, May 2005.
[10] F. S. Marzano, E. Fionda, and P. Ciotti, "Neural-network approach to ground-based passive microwave estimation of precipitation intensity and extinction," *J. Hydrol.*, vol. 328, pp. 121–131, 2006.
[11] C. Mätzler and J. Morland, "Advances in surface-based radiometry of atmospheric water," Inst. angewandte Physik, Univ. Bern, Bern, Switzerland, Tech. Rep. 2008-02-MW, 2008. iAP Res. Rep.
[12] H. Czekala, S. Crewell, C. Simmer, and A. Thiele, "Discrimination of cloud and rain liquid water path by ground based polarized microwave radiometry," *Geophys. Res. Lett.*, vol. 28, no. 2, pp. 267–270, 2001.
[13] H. Czekala, S. Crewell, A. Hornbostel, A. Schroth, C. Simmer, and A. Thiele, "Interpretation of polarization features in ground-based microwave observations as caused by horizontally aligned oblate raindrops," *J. Appl. Meteorol.*, vol. 40, no. 11, pp. 1918–1932, Nov. 2001.
[14] V. Wulfmeyer, A. Behrendt, H.-S. Bauer, C. Kottmeier, U. Corsmeier, A. Blyth, G. Craig, U. Schumann, M. Hagen, S. Crewell, P. Di Girolamo, C. Flamant, M. Miller, A. Montani, S. Mobbs, E. Richard, M. W. Rotach, M. Arpagaus, H. Russchenberg, P. Schlüssel, M. König, V. Gärtner, R. Steinacker, M. Dorninger, D.D. Turner, T. Weckwerth, A. Hense, and C. Simmer, "The convective and orographically-induced precipitation study: A research and development project of the world weather research program for improving quantitative precipitation forecasting in low-mountain regions," *Bull. Amer. Meteorol. Soc.*, vol. 89, no. 10, pp. 1477–1486, 2008.
[15] A. Battaglia, C. Simmer, and H. Czekala, "Three-dimensional effects in polarization signatures as observed from precipitating clouds by low frequency ground-based microwave radiometers," *Atmos. Chem. Phys.*, vol. 6, no. 12, pp. 4383–4394, 2006.
[16] K. Andsager, K. V. Beard, and N. S. Laird, "A laboratory study of oscillations and axis ratios for large raindrops," *J. Atmos. Sci.*, vol. 56, pp. 2673–2683, 1999.
[17] M. I. Mishchenko, "Calculation of the amplitude matrix for a nonspherical particle in a fixed orientation," *Appl. Opt.*, vol. 39, no. 6, pp. 1026–1031, Feb. 2000.
[18] A. Battaglia, C. Davis, C. Emde, and C. Simmer, "Microwave radiative transfer intercomparison study for 3-D dichroic media," *J. Quant. Spectrosc. Radiat. Transf.*, vol. 105, no. 1, pp. 55–67, May 2007.
[19] A. Battaglia, C. Kummerow, D.-B. Shin, and C. Williams, "Toward characterizing the effect of radar bright bands on microwave brightness temperatures," *J. Atmos. Ocean Technol.*, vol. 20, no. 6, pp. 856–871, 2003.